Published in final edited form as:
Opt Express. 2007 December 10; 15(25): 16922–16932.

Simultaneous SLO/OCT imaging of the human retina with axial eye motion correction

Michael Pircher, **Bernhard Baumann**, **Erich Götzinger**, **Harald Sattmann**, and **Christoph K. Hitzenberger**
Center for Biomedical Engineering and Physics, Medical University of Vienna

Abstract

It has been shown that transversal scanning (or en-face) optical coherence tomography (TS-OCT) represents an imaging modality capable to record high isotropic resolution images of the human retina in vivo. However, axial eye motion still remains a challenging problem of this technique. In this paper we introduce a novel method to compensate for this eye motion. An auxiliary spectral domain partial coherence interferometer (SD-PCI) was integrated into an existing TS-OCT system and used to measure accurately the position of the cornea. A light source emitting at 1310nm was used in the additional interferometer which enabled a nearly loss free coupling of the two measurement beams via a dichroic mirror. The recorded corneal position was used to drive an additional voice coil translation stage in the reference arm of the TS-OCT system to correct for axial eye motion. Currently, the correction can be performed with an update rate of ~200Hz. The TS-OCT instrument is operated with a line scan rate of 4000 transversal lines per second which enables simultaneous SLO/OCT imaging at a frame rate of 40fps. 3D data of the human retina with isotropic high resolution, that was sufficient to visualize the human cone mosaic in vivo, is presented.

1. Introduction

To image the living human retina on a cellular level still remains a major challenge for ophthalmic instruments. In the recent decades two imaging techniques have been introduced to the field that improved resolution. Optical coherence tomography (OCT) [1,2] and adaptive optics (AO) enhanced ophthalmic instruments (e.g. fundus photography [3] or scanning laser ophthalmoscopy (SLO) [4]). The first technique provides unprecedented depth resolution with a rather moderate transverse resolution. Further improvement of OCT technology was introduced with the demonstration of a sensitivity advantage of Fourier Domain OCT (FD-OCT) compared to standard time domain OCT (TD-OCT) techniques [5, 6]. This dramatically increased imaging speed, enabling to record 3D data of the human retina in vivo [7]. AO enhanced instruments provide excellent (nearly diffraction limited) transverse resolution which enabled the visualization of cone photoreceptors in the living human retina. However, depth resolution of this technique is determined by the confocal gate and is limited by the optics of the eye to 50 to 100μm [4]. Only very recently a combination of OCT with AO has been introduced to improve resolution in all dimensions, and the capability of these instruments to resolve individual retinal cones in vivo in OCT B-scans has been demonstrated [8, 9].

---

michael.pircher@meduniwien.ac.at.

OCIS codes: (170.4500) Optical Coherence Tomography; (120.3890) Medical optics instrumentation; (170.4460) Ophthalmic Optics; (170.4470) Ophthalmology.

However, since most of these instruments are based on recording A-scans (i.e. the fast or priority scan direction is in depth) several problems remain: To retrieve en-face information, a whole 3D data set has to be recorded. This is rather time consuming and motion artifacts in transverse direction are most likely to be observed. Two methods have been proposed to reduce these artifacts. The first method uses a greatly reduced scanning area of 38 × 19 μm^2 or 38 × 285 μm^2 [10]. A second method uses a post-processing algorithm which yields very good results for larger structures, however small features as the human cone mosaic remain distorted [11]. Another problem inherent in high transverse resolution OCT systems is the limited depth of field or depth of focus (DOF). Only a small depth range within the retinal image will be in focus. To obtain data of high transverse resolution throughout the retina several 3D data sets with shifted focus have to be recorded and merged to obtain a whole volume of the retina with high isotropic resolution.

Transversal scanning (or en-face) optical coherence tomography (TS-OCT) represents an alternative imaging scheme [12]. In this technique the fast or priority scan direction is perpendicular to the imaging beam. Therefore, en-face images can be recorded very rapidly which minimizes transverse motion artifacts. Another advantage of this technique is the possibility to record simultaneously SLO images [13, 14] and the possibility to implement a dynamic shift of focus to maintain high transverse resolution throughout imaging depth [15]. The capability of TS-OCT for ophthalmic imaging was demonstrated in pathologies [16], for high speed imaging [17], polarization sensitive imaging [17, 19] and ultrahigh resolution imaging [20] and in combination with adaptive optics [21]. Recently, we reported on imaging the human cone mosaic in vivo with SLO and OCT without AO [22].

Motion artifacts caused by involuntary axial (in depth) eye movement (or by involuntary head motion) remains a challenging problem of this technique. In this paper we introduce, based on our previously published TS-OCT instrument [22] a new development which includes the improvement of measurement speed and a new method to measure and correct for axial motion of the eye. The idea is to use the corneal reflex as a reference signal to determine the depth position of the eye. This signal is then used to drive a translation stage in the reference arm of the TS-OCT system to correct for eye motion. The simultaneously recorded SLO channel enabled a correction for transverse eye motion in a post processing step via software. 3D data of a human retina recorded with the new technique is presented.

2. Methods

2.1 Experimental configuration

The experimental setup is shown in Fig. 1. The instrument consists of two separated parts: A high speed TS-OCT system operating at 840nm, and a spectral domain (SD) partial coherence interferometer (PCI) operating at 1310nm. The TS-OCT part is based on our previous system [22]. In brief, a Mach Zehnder interferometer is used with a light source of 50nm bandwidth that results in a depth resolution of ~6μm in air. The collimated light is horizontally linear polarized and is split into a reference beam and a sample beam at the first non-polarizing beam splitter (BS-1). The light in the sample arm traverses dispersion compensation glass rods (not shown in Fig. 1) and is directed by a second non polarizing beam splitter (BS-2) to a x-y scanning unit consisting of a resonant scanner operating at a scanning frequency of 4 kHz (x-direction) and a galvo scanner (y-direction). A telescope images the pivot point of the resonant scanner into the pupil plane of the eye. The second lens (L2) is mounted on a translation stage which enables a simultaneous shift of the focal plane with the coherence gate (dynamic focus) during measurement [15]. On the way back, scattered light from the retina is split into two parts by BS-2. The first part is directed to the final non-polarizing beam splitter (BS-3) at the interferometer exit and is recombined with light from the reference arm. The second part traverses the first beam splitter (BS-1) and is detected by an additional detector which enables a simultaneous recording of a SLO signal. In the reference arm a carrier frequency is introduced to the coherence signal by implementing two acousto optic modulators (AOM's). The frequency shift of the AOM's was set to −40MHz and +41MHz respectively, which resulted in a net frequency shift of 1MHz. A translation stage placed in the reference arm enables depth scanning. Additionally, glass prisms (not shown in Fig. 1) are placed in the reference arm to compensate for residual interferometer dispersion and dispersion introduced by the eye. To correct for axial eye motion a fast voice coil translation stage (Physik Instrumente, V-102) is mounted on top of the first translation stage. The recombined light from both interferometer exits was directed to a balanced receiver, amplified and recorded with a data acquisition board. Data is processed with a standard personal computer (PC). Two different fast imaging modes can be used with this instrument: B-scan mode (x-z imaging plane) and C-scan mode (x-y imaging plane). We used a power of 700μW on the cornea which is well below the laser safety limits for this wavelength region. The instrument is currently operated at a frame rate of 40 fps, each frame consisting of 650 (x) × 100 (y) pixels. Only one scan direction of the resonant scanner is used.

The second part is marked with a black rectangle in Fig. 1 and shows the auxiliary fiber based SD-PCI that was operated with a light source of 55nm bandwidth resulting in a depth resolution of ~14μm. Note that the position of the cornea can be determined with higher precision since only the signal from one interface (reflex) is used and the peak of the resulting coherence function can be measured more accurately. The collimated beam from the sample arm of the SD-PCI was coupled into the measurement arm of the TS-OCT system via a dichroic mirror to minimize losses in both systems. The spectrometer of the SD-PCI system incorporates a grating (830 lines per mm) and a 1024 pixels InGaAs camera. The exposure time of the camera was set to 200μs resulting in an A-scan rate of 5000/s. The camera output was recorded with a data acquisition board implemented in an additional PC. Before Fourier transformation of the recorded spectral data the standard procedures to enhance signal to noise ratio were performed (i.e. subtracting of reference spectrum and rescaling). The position of the corneal signal (note that a collimated beam is used, hence no internal structure but a reflex at the corneal surface can be observed) is determined very accurately via a peak detection algorithm. This position is used to drive a voice coil translation stage in the reference arm of the TS-OCT system. The correction was running independently from the TS-OCT system and the update time for the correcting signal was ~5ms. The closed loop depth correction system is operated with a simple proportional control algorithm and the step response time of the voice coil translation stage provided by the manufacturer is 30 to 60ms.

2.2 Data recording and post processing

The patient was placed on a chin rest. No bite bar was used for all of the measurements. The instrument can be operated in two different imaging modalities: B-scan mode (y-scanner held on a fixed position) and C-scan mode. The latter mode was used to record 3D data that consisted of 120 C-scans in 3 seconds. In this mode the translation stage was moved at a constant speed. The scanning angle on the retina in x and y direction was ~0.8°. Simultaneous to the depth scanning the focal plane was shifted in depth by moving lens L2 to maintain the high transverse resolution. A detailed description of the dynamic focus can be found in reference [15]. 6 channels were recorded simultaneously during measurement: SLO channel, OCT channel, y-scanner position, x-scanner scanning direction, measured corneal position and the position of the voice coil translation stage. After data recording, the signals from SLO channel and OCT channel, respectively, were cut into individual C-scans with the use of the y-scanner position and x-scanner scanning direction. Each transversal line (x-direction) was corrected for distortions caused by the sinusoidal motion of the resonant scanner. Because of the fast imaging capability of our instrument we can use the simultaneously recorded SLO images to correct for transverse retinal motion. For this purpose we used an algorithm described in Ref. [23]. To maintain a pixel to pixel correspondence between SLO and OCT channel, respectively, we combined both images (represented in an 8 bit format) into a red-green-blue (RGB) image before applying the transverse motion correction algorithm. All presented data has been corrected with this post processing algorithm to correct for transverse motion. After motion correction the data set was re-sampled into 256×256×120 pixels to provide equal sampling density in x-y-direction.

3. Results

3.1 Performance of axial eye motion correction

Figure 2 shows an example of the recorded corneal position evolving in time during a 3D measurement with the TS-OCT system. The black line corresponds to the measured axial position of the corneal apex; the red line corresponds to the position of the voice coil translation stage. Clearly visible are fast oscillations and a slower drift of the corneal position. Figure 2(b) shows the difference between measured corneal position and voice coil translation stage position. Most of the oscillations are reduced and a slower drift in depth could be eliminated. However, because of the inertia of the used correcting translation stage, a residual tracking error (in the order of 10-20μm) remains. From these figures we calculated without motion correction a mean deviation from zero position of the cornea of 30μm with a standard deviation of 26μm. The current correction procedure reduced the mean deviation to 0μm with a standard deviation of ~6μm. From Fig. 2(a) we could estimate the closed loop bandwidth of our system by measuring the delay of the voice coil translation stage position from the actual position of the cornea at 10 different time points. For this measurement we chose positions of rapid excursions and measured a mean delay of 20ms which corresponds to a closed loop bandwidth of 50Hz.

To test the performance of the axial position correction during TS-OCT imaging we imaged the retina of a healthy volunteer. 120 en-face images were recorded while the translation stage (used for depth scanning) was kept at a fixed position that corresponded to a depth position at the en-face imaging plane within the retina of the junction between inner and outer segments of photoreceptors (IS/OS). The left hand side of Fig. 3 shows a sequence of en-face images with no correction (voice coil translation stage kept at a fixed position) and the right hand side of the image shows a sequence with the correction turned on. In the uncorrected case a permanent axial motion of the imaging plane is clearly visible (an example for axial motion is shown in Fig. 2(a), and therefore the retinal plane of interest (IS/OS) is not visible most of the time. With the correction turned on, the imaging plane is visible throughout measurement time, and only small variations in depth are visible due to the residual tracking error (c.f. Fig. 2(b)) caused by the inertia of the voice coil translation stage.

3.2 Motion corrected imaging of the human retina

To clarify the labeling of the different retinal layers used in this paper, Fig. 4 shows a high isotropic resolution B-scan recorded with the instrument. All retinal layers which can be seen with UHR-OCT can be observed. Differing labeling has been reported with respect to the posterior layers. We used the following labeling of the posterior four bright layers (c.f. Fig. 4): external limiting membrane (ELM), junction between inner and outer segments of photoreceptors (IS/OS), end tips of photoreceptors (ETPR) or Verhoeff’s membrane, and retinal pigment epithelium (RPE). Note that the regular spacing within the IS/OS and ETPR layer is not very pronounced within the image because the image is displayed on a logarithmic grey scale in order to reduce the high dynamic range of the OCT image.

Figure 5 shows a motion corrected 3D data set (fly through movie) recorded with the new depth position correction at an eccentricity of ~3° to 4° nasally to the fovea. The left hand side shows SLO images, the center shows en-face OCT images and the right hand side shows OCT B-scan images. Note that the OCT images are represented on a logarithmic scale and the SLO images are represented on a linear scale. To reduce the amount of data the first 40 frames (corresponding to imaging planes within the vitreous of the eye) of the 3D-data set are omitted. Therefore the image sequence starts at a depth position of the inner limiting membrane (ILM) and proceeds from the inner retina to the outer retina. Within the SLO images the shift of focus can be clearly observed. In the first frames the retinal nerve fiber layer (RNFL) appears sharp whereas in the following frames the photoreceptors come into focus and start to blur in the final frames of the movie.

When comparing the SLO and en-face OCT images the parallel shift of focus with the coherence gate can be observed. Note that the best sharpness of the RNFL and cone photoreceptors observed in the SLO images coincides with the corresponding layers in the en-face OCT images. The superior depth resolution of OCT enables the separation and visualization of the ILM, RNFL bundles, capillaries within the GCL, INL and the cone mosaic within the IS/OS junction and the ETPR layer. To identify the individual layers a white line in OCT B-scan image marks the corresponding position of the en-face image. A white line in the en-face OCT images marks the corresponding position of the OCT B-scan. Interestingly, cone like structures can be observed in the space between the layers of IS/OS and ETPR (visible in frames 41 to 44 of the en-face OCT movie). Note that this observation can be made within the en-face OCT images as well as within the B-scan images (visible e.g. in frames 15 and 16 of the B-scan movie between IS/OS junction and ETPR layer). Due to the transverse motion correction algorithm black horizontal bars are appearing at the beginning and the end of each image sequence.

Figure 6 shows a comparison of the cone mosaic imaged with SLO and OCT. For the OCT images the signal was squared (OCT measures the amplitude of the light, SLO the intensity) and displayed on a linear scale to enable a direct comparison between both imaging modalities. To enhance signal to noise ratio the SLO image was averaged over 10 successive frames. Within this image the cone mosaic can be clearly observed (c.f. Fig. 6(a)). To measure the (closest neighbor) cone spacing, we calculated a 2D FFT of this image and measured the radius of the resulting ring, a procedure described in detail in Ref. [24]. With this procedure we calculated for this eccentricity a cone spacing of ~1.47 arcminutes or ~7μm (if we assume that 1° corresponds to 292μm on the retina). This is in good agreement with values obtained from histology [25]. Figure 6(b) shows the corresponding OCT data averaged over the same number of frames (equivalent to an optical depth of ~80 μm) resulting in a speckle reduced image. Both images are very similar emphasizing the pixel to pixel correspondence between SLO and OCT. However, the cone mosaic extracted from the ETPR and the IS/OS junction, respectively appears different because speckles are more pronounced in these images (c.f. Figs. 6(c) and 6(d)). Even though most of the individual cones can be resolved and identified in the SLO image, speckles distort some of the small features in the OCT images. However, the reflection sites of the IS/OS and ETPR layers might not be exactly within one plane, therefore some maxima of the individual coherence functions are deviating from the imaging (or coherence) plane leading to varying intensities of these reflection sites within the image. This further leads to a different appearance of the cone mosaic in the SLO and OCT images.

Figure 7 shows different imaging planes extracted from the 3D OCT data set. All images are displayed on a linear scale. Figure 7(a) shows an imaging plane corresponding to the ILM. Because the imaging plane does not totally coincide with the ILM which is very thin, this layer is visible mainly in the left part of the image. Figure 7(b) shows an imaging plane corresponding to the RNFL. Clearly visible are the nerve fiber bundles extending almost horizontally within the image. Recently, similar images have been presented with the use of AO-OCT [11]. The visualization of capillaries is more difficult because theses structures generally have a three dimensional extension. Therefore only part of the structure will be visible within one en-face image. However, the signal intensity obtained from capillaries is very high. Therefore we searched within a specific layer (e.g. GCL, INL) for the maximum signal along an A-line (in depth). The result is displayed in Figs. 7(c) and 7(d), respectively. The 2 dimensional structures of the capillaries can be clearly observed. From these images we estimate the thickness of the smallest capillary (vertical capillary on the left hand side of Fig. 7(c)) to ~5μm. Note that in Fig. 7(d) the shadows of the capillaries of Fig. 7(c) are faintly visible. The appearance of the capillaries (separation into small spots) might give the impression that individual cells within the capillaries can be resolved, however speckles might cause a similar appearance, therefore we think that further investigations (e.g. temporal evolution of these spots) are necessary to clarify this point.

4. Discussion

In this paper we introduced a method for TS-OCT to overcome the problem of motion artifacts in depth, up to now a major limitation of the technique. As shown in Fig. 2 depth motion can be separated into two parts: a slow drift of a mean position in one direction and rapid oscillations around this mean position in both directions. The first part could be completely eliminated with our method while influence of the second part could be greatly reduced. Depth control is not only valuable during data recording but very important for the correct alignment of the dynamic focus (i.e. to match the confocal plane with the coherence gate) [15]. In this case it is sufficient to correct for the slow drift because the depth of field is in the order of 60-100μm which is larger than the small oscillations. However, to obtain more accurate depth information it is essential to correct the small oscillations as well. Currently the inertia of the used translation stage limits the performance of our system. Therefore, a residual tracking error in the order of 10-20μm remains. Although this error is in the range of the sampling density of the presented data (~10μm) higher precision should be possible with the implementation of a faster translation stage or a rapid scanning optical delay line [26, 27].

Our technique requires a fixed distance between measured corneal position and retinal position. The correction method can not distinguish between a change of this distance and eye motion in depth. Fundus pulsation is in the order of a few microns [29] (i.e. below the axial resolution of the instrument) and can therefore be neglected in the current state of development. A more detailed analysis of the influence of fundus pulsation might become necessary if ultra high resolution imaging would be implemented. Another possible change of distance might be introduced by transverse eye motion because of the curvature of the cornea. However, we choose a parallel beam incident on the cornea to measure the corneal position. Therefore transverse motion will result in a decrease of signal strength (only part of the beam which is backreflected contributes to the signal) not in a change of depth position as described in detail in reference [30]. More problematic is rotation of the eye. Because the radius of the exterior corneal curvature generally does not match the distance between corneal surface and axis of rotation, a change in the distance between cornea and retina caused by the rotation of the eye is expected. However, we calculated that the error of depth position even for a rotation of ~1° (larger than the field of view) for the measured volunteer (measured corneal radius ~7.2mm, measured eye length ~25mm) is smaller than 1.5μm. This is well below the resolution of the system and can therefore be neglected.

Since the discovery of a sensitivity advantage of FD-OCT compared to time domain OCT, the latter was more and more regarded as obsolete. However, as we showed in this paper, transversal scanning OCT, a variant of time domain OCT, provides some advantages especially for high transverse resolution systems that are not (yet) accessible with FD-OCT. 1) Dynamic focus: To maintain high transverse resolution throughout imaging depth the focus has to be moved parallel to the coherence gate. In this paper we demonstrated the performance of a dynamic focus in TS-OCT. Since in FD-OCT the whole depth is recorded instantaneously (with one shot) a dynamic focus is not possible. However, it should be mentioned that efforts are made to overcome this limitation by the use of special illumination beams (e.g. Bessel beams) [28]. But these methods suffer from a tremendous loss of sensitivity (decreasing the benefit of FD-OCT) and have not been demonstrated on the living human eye. 2) Correction of transverse eye motion: To resolve small details as the human cone mosaic transverse eye motion has to be corrected. In TS-OCT the fast scanning direction is perpendicular to the imaging beam and en-face images can be recorded very rapidly. This greatly reduces motion artifacts within a frame. As we showed in this paper the signal from the SLO channel can be used to correct for transverse motion which further reduces artifacts caused by eye motion. In FD-OCT en-face information is usually extracted from a 3D-data set that is rather time consuming. Therefore, transverse eye motion artifacts will be more pronounced. Although post processing algorithms can be used to reduce these artifacts [11], residual errors that distort structures of interest (e.g. the human cone mosaic) remain. Retinal tracker might be used to correct for transverse motion [31, 32], however, these methods have not yet been demonstrated in combination with FD-OCT with the high accuracy needed for cellular imaging.

5. Conclusion

We presented a method to compensate for axial eye motion in transverse scanning OCT. We demonstrated the ability of the instrument to record 3D data of the human retina in vivo with high resolution. Using a dynamic focus enabled the maintenance of the high transverse resolution through imaging depth. Transverse motion was corrected using SLO images that were acquired simultaneously to the OCT images. The transverse resolution of the system was sufficient to resolve the human cone mosaic at an eccentricity of ~3° to 4° nasally of the fovea. Furthermore, we presented a direct comparison of cone mosaic images obtained with SLO and OCT and demonstrated the visualization of the ILM, RNFL bundles, and capillaries in the inner retina.

Acknowledgments

Financial assistance from the Austrian Fonds zur Förderung der wissenschaftlichen Forschung (FWF-grant P16776-N02) is gratefully acknowledged

References and links

1. Huang D, Swanson EA, Lin CP, Schuman JS, Stinson WG, Chang W, Hee MR, Flotte T, Gregory K, Puliafito CA, Fujimoto JG. Optical coherence tomography. Science. 1991; 254:1178–1181. [PubMed: 1957169]
2. Fercher AF, Hitzenberger CK, Drexler W, Kamp G, Sattmann H. In-vivo optical coherence tomography. Am. J. Ophthalmol. 1993; 116:113–115. [PubMed: 8328536]
3. Liang J, Williams DR, Miller DT. Supernormal vision and high-resolution retinal imaging through adaptive optics. J. Opt. Soc. Am. A. 1997; 14:2884–2892.
4. Roorda A, Romero-Borja F, Donnelly WJ, Queener H, Hebert TJ, Campbell MCW. Adaptive optics scanning laser ophthalmoscopy. Opt. Express. 2002; 10:405–412. http://www.opticsinfobase.org/abstract.cfm?URI=oe-10-9-405. [PubMed: 19436374]
5. Leitgeb RA, Hitzenberger CK, Fercher AF. Performance of Fourier domain vs. time domain optical coherence tomography. Opt. Express. 2003; 11:889–894. http://www.opticsinfobase.org/abstract.cfm?URI=oe-11-8-889. [PubMed: 19461802]

6. de Boer JF, Cense B, Park BH, Pierce MC, Tearney GJ, Bouma BE. Improved signal to noise ratio in spectral domain compared with time domain optical coherence tomography. Opt. Lett. 2003; 28:2067–2069. [PubMed: 14587817]
7. Wojtkowski M, Srinivasan V, Fujimoto JG, Ko T, Schuman JS, Kowalczyk A, Duker JS. Three-dimensional retinal imaging with high-speed ultrahigh-resolution optical coherence tomography. Ophthalmology. 2005; 112:1734–1746. [PubMed: 16140383]
8. Zhang Y, Rha J, Jonnal RS, Miller DT. Adaptive optics parallel spectral domain optical coherence tomography for imaging the living retina. Opt. Express. 2005; 13:4792–4811. http://www.opticsinfobase.org/abstract.cfm?URI=oe-13-12-4792. [PubMed: 19495398]
9. Zawadzki RJ, Jones SM, Olivier SS, Zhao M, Bower BA, Izatt JA, Choi S, Laut S, Werner JS. Adaptive-optics optical coherence tomography for high-resolution and high-speed 3D retinal in vivo imaging. Opt. Express. 2005; 13:8532–8546. http://www.opticsinfobase.org/abstract.cfm?URI=oe-13-21-8532. [PubMed: 19096728]
10. Zhang Y, Cense B, Rha J, Jonnal RS, Gao W, Zawadzki RJ, Werner JS, Jones S, Olivier S, Miller DT. High-speed volumetric imaging of cone photoreceptors with adaptive optics spectral-domain optical coherence tomography. Opt. Express. 2006; 14:4380–4394. http://www.opticsinfobase.org/abstract.cfm?URI=oe-14-10-4380. [PubMed: 19096730]
11. Zawadzki RJ, Choi SS, Jones SM, Oliver SS, Werner JS. Adaptive optics–optical coherence tomography: optimizing visualization of microscopic retinal structures in three dimensions. J. Opt. Soc. Am. A. 2007; 24:1373–1383.
12. Podoleanu AG, Dobre GM, Jackson DA. En-face coherence imaging using galvanometer scanner modulation. Opt. Lett. 1998; 23:147–149. [PubMed: 18084441]
13. Podoleanu, A. Gh.; Jackson, DA. Combined Optical Coherence Tomograph and Scanning Laser Ophthalmoscope. Electron. Lett. 1998; 34:1088–1090.
14. Podoleanu, A. Gh.; Jackson, DA. Noise Analysis of a Combined Optical Coherence Tomograph and a Confocal Scanning Ophthalmoscope. Appl. Opt. 1999; 38:2116–2127. [PubMed: 18319772]
15. Pircher M, Götzinger E, Hitzenberger CK. Dynamic focus in optical coherence tomography for retinal imaging. J. Biomed. Opt. 2006; 11:054013. [PubMed: 17092162]
16. van Velthoven MEJ, Verbraak FD, Garcia PM, Schlingemann RO, Rosen RB, de Smet MD. Evaluation of central serous retinopathy with en face optical coherence tomography. Br. J. Opthalmol. 2005; 89:1483–1488.
17. Hitzenberger CK, Trost P, Lo PW, Zhou Q. Three dimensional imaging of the human retina by high speed optical coherence tomography. Opt. Express. 2003; 11:2753–2761. http://www.opticsinfobase.org/abstract.cfm?URI=oe-11-21-2753. [PubMed: 19471390]
18. Pircher M, Götzinger E, Leitgeb R, Sattmann H, Findl O, Hitzenberger CK. Imaging of polarization properties of human retina in vivo with phase resolved transversal PS-OCT. Opt. Express. 2004; 12:5940–5951. http://www.opticsinfobase.org/abstract.cfm?URI=oe-12-24-5940. [PubMed: 19488235]
19. Pircher M, Götzinger E, Findl O, Michels S, Geitzenauer W, Leydolt C, Schmidt-Erfurth U, Hitzenberger CK. Human macula investigated in vivo with polarization sensitive optical coherence tomography. Invest. Ophthalmol. Visual. Sci. 2006; 47:5487–5494. [PubMed: 17122140]
20. Pircher M, Goetzinger E, Leitgeb RA, Sattmann H, Hitzenberger CK. Ultrahigh resolution polarization sensitive optical coherence tomography. SPIE Proceeding. 2005; 5690:257–262.
21. Merino D, Dainty C, Bradu A, Podoleanu Adrian Gh. Adaptive optics enhanced simultaneous *en-face* optical coherence tomography and scanning laser ophthalmoscopy. Opt. Express. 2006; 14:3345–3353. http://www.opticsinfobase.org/abstract.cfm?URI=oe-14-8-3345. [PubMed: 19516479]
22. Pircher M, Baumann B, Götzinger E, Hitzenberger CK. Retinal cone mosaic imaged with transversal scanning OCT. Opt. Lett. 2006; 31:1821–1823. [PubMed: 16729082]
23. Thevenaz P, Ruttimann UE, Unser M. A pyramid approach to subpixel registration based on intensity. IEEE Trans. Image Process. 1998; 7:7–41.
24. Pircher M, Zawadzki RJ, Evans JW, Werner JS, Hitzenberger CK. Simultaneous imaging of human cone mosaic with adaptive optics enhanced scanning laser ophthalmoscopy and high-speed transversal scanning optical coherence tomography. Opt. Lett. 2007 in press.

25. Curcio CA, Sloan KR, Kalina RE, Hendrickson AE. Human photoreceptor topography. J. Compar. Neurol. 1990; 292:497–523.
26. Tearney GJ, Bouma BE, Fujimoto JG. High-speed phase- and group-delay scanning with a grating-based phase control delay line. Opt. Lett. 1997; 22:1811–1813. [PubMed: 18188374]
27. Iftimia N, Bouma B, de Boer J, Park B, Cense B, Tearney G. Adaptive ranging for optical coherence tomography. Opt. Express. 2004; 12:4025–4034. http://www.opticsinfobase.org/abstract.cfm?URI=oe-12-17-4025. [PubMed: 19483942]
28. Leitgeb RA, Villiger M, Bachmann AH, Steinmann L, Lasser T. Extended focus depth for Fourier domain optical coherence microscopy. Opt. Lett. 2006; 31:2450–2452. [PubMed: 16880852]
29. Schmetterer L, Dallinger S, Findl O, Strenn K, Graselli U, Eichler HG, Wolzt M. Noninvasive investigations of the normal ocular circulation in humans. Invest. Ophthalmol. Visual Sci. 1998; 39:1210–1220. [PubMed: 9620081]
30. Hitzenberger CK. Measurement of corneal thickness by low-coherence interferometry. Appl. Opt. 1992; 31:6637–6642. [PubMed: 20733890]
31. Hammer DX, Ferguson RD, Magill JC, White MA, Elsner AE, Webb RH. Compact scanning laser ophthalmoscope with high-speed retinal tracker. Appl. Opt. 2003; 42:4621–4632. [PubMed: 12916631]
32. Hammer DX, Ferguson RD, Bigelow CE, Iftimia NV, Ustun TE, Burns SA. Adaptive optics scanning laser ophthalmoscope for stabilized retinal imaging. Opt. Express. 2006; 14:3354–3367. http://www.opticsinfobase.org/abstract.cfm?URI=oe-14-8-3354. [PubMed: 19516480]

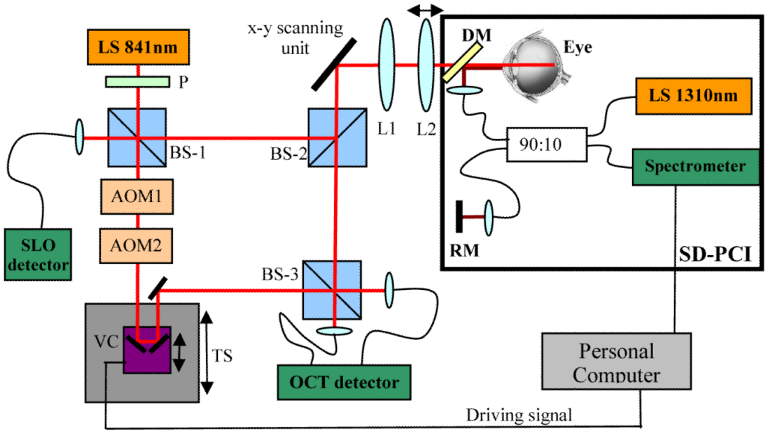

Fig. 1.

Sketch of the experimental setup. L1 fixed lens, L2 lens mounted on a translation stage, DM dichroic mirror, RM reference mirror, TS translation stage, VC voice coil translation stage, LS light source, AOM acousto optic modulator, P polarizer, BS non polarizing beam splitter

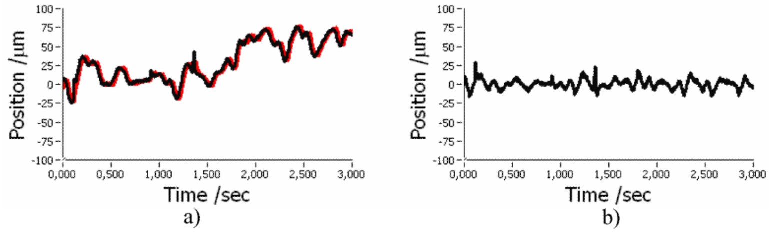

Fig. 2.

Performance of axial eye motion correction. a) Black…recorded corneal position, red… motor position b) difference between curves in a)

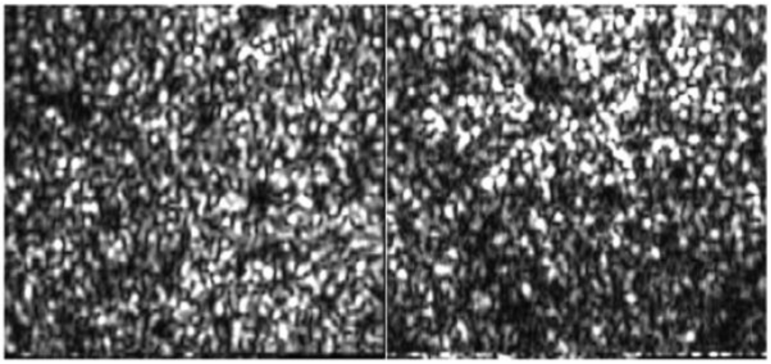

Fig. 3.

Frame No. 8 of a sequence of en-face images recorded at fixed position of the translation stage. Left side: without depth correction. Right side: correction turned on. Field of view: 0.8°×0.8°. (To reduce file size, the pixel extension of the original movie was reduced by 70%; The bottom horizontal line is an artifact caused by the turning of the y-scanner.)

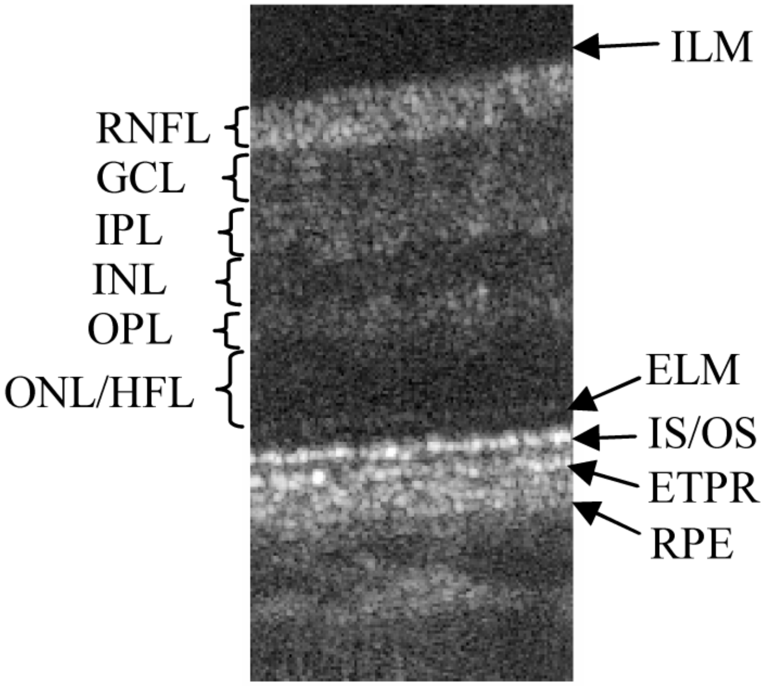

Fig. 4.

High resolution B-scan with axial motion correction turned on. (Extension: 0.8° × 670μm (optical)). ILM inner limiting membrane, RNFL retinal nerve fiber layer, GCL ganglion cell layer, IPL inner plexiform layer, INL inner nuclear layer, OPL outer plexiform layer, ONL/HFL outer nuclear layer/ Henle fiber layer, ELM external limiting membrane, IS/OS junction between inner and outer segments of photoreceptors, ETPR end tips of photoreceptors, RPE retinal pigment epithelium

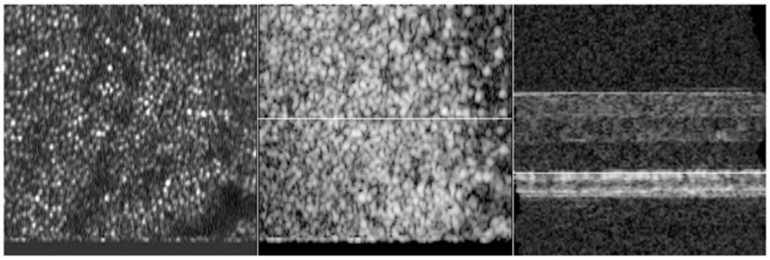

Fig. 5.

Frame No. 39 of a movie showing 3D data of the retina recorded with the instrument. Left side shows SLO images, the center shows en-face OCT images, right side shows extracted OCT B-scans. The white line shows the position of the corresponding B-scan (in the center image) and position of the corresponding en-face image (on the right hand side image), respectively. SLO images are displayed on a linear scale, OCT images are displayed on a logarithmic scale. Field of view of SLO and en-face OCT images: 0.8°×0.8°. Dimension of OCT B-scan: 0.8° × 1mm (To reduce file size, the pixel extension of the original movie was reduced by 70%)

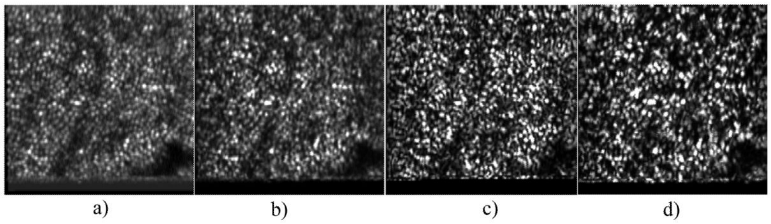

Fig. 6.

Comparison of the cone photoreceptor mosaic imaged with different imaging modalities. a) SLO image (averaged over 10 frames), b) OCT image (averaged over an optical depth of ~80μm), c) OCT retrieved from the ETPR layer, d) OCT retrieved from the IS/OS junction. Field of view of each image: 0.8°×0.8°. (For a better comparison with the SLO images all OCT images are squared and displayed on a linear scale)

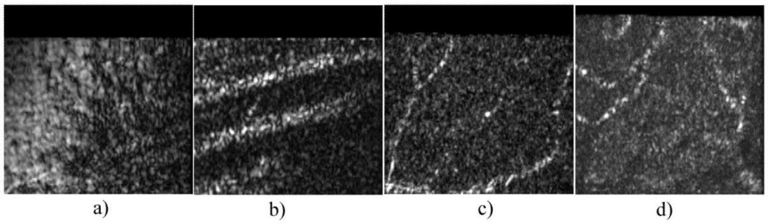

Fig. 7.

Imaging planes at different depths extracted from the OCT data. a) ILM, b) RNFL, c) GCL (maximum intensity within 4 frames), d) INL (maximum intensity within 7 frames) Field of view of each image: 0.8°×0.8°. (All images are displayed on a linear scale.)